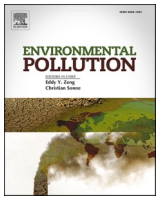
Environmental Pollution 386 (2025) 127213



Contents lists available at ScienceDirect

Environmental Pollution

journal homepage: www.elsevier.com/locate/envpol



Flux measurements of NO_x, O_3 and O_x: Emission characteristics, inventory validation and titration effects☆

Xiaoxiao Zhang [a], Bin Yuan [a,*], Yibo Huangfu [a], Huizhi Liu [b], Thomas Karl [c], Ming Chang [a], Shiyi Chen [d], Tao Song [e], Jintai Lin [f], Guannan Geng [g], Hongjuan Li [h], Eran Tas [i]

[a] College of Environmental and Climate, Institute for Environmental and Climate Research, Guangdong-Hongkong-Macau Joint Laboratory of Collaborative Innovation for Environmental Quality, Jinan University, 511443, Guangzhou, China
[b] Department of Atmospheric Sciences, Yunnan University, Kunming, 650091, China
[c] Department of Atmospheric and Cryospheric Sciences, University of Innsbruck, Innsbruck, Austria
[d] State Key Joint Laboratory of Environment Simulation and Pollution Control, College of Environmental Sciences and Engineering, Peking University, Beijing, 100871, China
[e] State Key Laboratory of Atmospheric Boundary Layer Physics and Atmospheric Chemistry, Institute of Atmospheric Physics, Chinese Academy of Sciences, Beijing, 100029, China
[f] Laboratory for Climate and Ocean-Atmosphere Studies, Department of Atmospheric and Oceanic Sciences, School of Physics, Peking University, Beijing, 100871, China
[g] State Key Laboratory of Regional Environment and Sustainability, School of Environment, Tsinghua University, Beijing, 100084, China
[h] Beijing Aozuo Ecological Instrument Co., Ltd, Beijing, 101160, China
[i] Institute of Environmental Sciences, Soil and Water Department, The Hebrew University of Jerusalem, Israel

ARTICLE INFO

Keywords:
NO_x
Flux
Traffic flow
Emission inventory
Titration effect
O_3 downward flux

ABSTRACT

As the precursor of ozone and secondary particles, the incomplete knowledge of NO_x emission dynamics constrains our ability to fully elucidate air pollution formation. Flux measurements offer new insights into NO_x emissions and titration effects. Here, we present eddy covariance flux measurements of NO_x, O_3 and O_x in urban Beijing during the summer of 2023. The measured NO_x flux was positive with the 24-h average of 10.4 ± 10.7 nmol/m^2/s, which is at the lower end of the flux reported in urban regions. The low NO_x emission strength in urban Beijing may be related to the successful control measures of diesel vehicles, while confirming significant dependence of NO_x flux with traffic flow. The discrepancies by a factor of 1.3–14.5 between measured NO_x flux and estimates in emission inventories are observed, indicating most emission inventories may fail to accurately characterize NO_x emissions in Beijing. Better agreements between flux measurements and satellite retrieval are obtained. In contrast to NO_x, predominantly downward fluxes were observed for ozone (O_3) and O_x (=O_3 + NO_2). A multiple linear regression (MLR) method is developed to examine the impacts of NO_x emissions on the ozone downward flux, revealing that NO_x emissions induce 54 ± 53 % of ozone downward flux average over the observation period. This study demonstrates valuable information on emission strength and chemical transformation provided by eddy covariance flux measurements of NO_x, O_3 and O_x.

1. Introduction

Nitrogen oxides (NO_x = NO + NO_2) pose dual environmental threats through direct ecological and health impacts, and act as key precursors in atmospheric photochemistry (de Vries, 2021; Liu and Shi, 2021; Song et al., 2023; Wang et al., 2017). In China, atmospheric NO_x rosed markedly before 2011 due to industrialization and fossil fuel dependence (Jiang et al., 2022), but declined post 2012 following national controls (fossil fuel reductions, renewable energy expansion, etc.) (Jiang et al., 2022; Liu et al., 2016).

Projecting future NO_x is vital for air quality management, yet discrepancies between inventory simulations and observations persist (Hood et al., 2018; Kim et al., 2013; Zhao et al., 2018a), revealing fundamental inventory uncertainties. Hence, validation of emission inventory is critical in continuously reducing the uncertainties of emission estimates. Emission inventories are widely compared with modelling

☆ This paper has been recommended for acceptance by: Dr Alessandra De Marco.
* Corresponding author.
E-mail address: byuan@jnu.edu.cn (B. Yuan).

https://doi.org/10.1016/j.envpol.2025.127213
Received 8 August 2025; Received in revised form 18 September 2025; Accepted 3 October 2025
Available online 6 October 2025
0269-7491/© 2025 Elsevier Ltd. All rights are reserved, including those for text and data mining, AI training, and similar technologies.

inversions constrained by concentration measurements of targeted pollutants, collected either on the ground (Lamsal et al., 2014; Wang et al., 2011), aircraft (Hiller et al., 2014; Stockwell et al., 2022) or satellite (Kemball-Cook et al., 2015; Zhao et al., 2018b). Flux measurements through various techniques, including surface gradient method, eddy covariance method and relaxed eddy accumulation (REA) method, can be directly used to compare with emission inventory and provide direction to further improve the emission estimates (Desjardins et al., 2018; Mo et al., 2020; Pfannerstill et al., 2023). However, NO_x flux studies focus mainly on natural ecosystems (e.g. soil, grassland, forests etc.), while urban flux measurements remain scarce due to surface complexity, with documented cases limited to few cities like London in UK, Innsbruck in Austria, Beijing in China, Los Angeles, San Joaquin Valley, and Norfolk in U.S. (Cliff et al., 2025; Karl et al., 2023; Marr et al., 2013; Nussbaumer et al., 2023; Squires et al., 2020; Zhu et al., 2023). This limits the understanding of urban NO_x emission characteristics and NO-NO_2-O_3 interconversion.

Understanding the titration effect of NO_x is crucial for accurate urban ozone prediction, yet concentration-based methods suffer from complex couplings among meteorology, precursors, and photochemistry (Handisides et al., 2003; Liu and Shi, 2021). For instance, Ma et al. (2017) and Tadic et al. (2020) demonstrated that peroxy radicals competition with titration reactions induces a 60–80 % positive deviation from the NO-NO_2-O_3 photostationary state. Khalil (2018) showed that regional O_3 transport critically modulates the titration reactions. These studies show that isolating titration effects using concentration-based methods remains challenging under complex atmospheric conditions. Flux measurements offer new insight for investigating the titration effect. Karl et al. (2023) showed NO_x emissions affect ozone deposition via titration, with deposition fluxes being minor relative to NO + O_3 reaction fluxes. Given urban heterogeneity, validating this pattern across settings is essential, highlighting the need for broader urban NO_x and O_3 flux measurements.

As a megacity, Beijing regularly experiences ozone and particle pollution linked to NO_x emissions. Here, we present the first comprehensive NO_x, O_3 and O_x (=NO_2 + O_3) flux measurements using eddy covariance at an urban meteorological tower in Beijing during May–June 2023. The emission characteristics of NO_x in Beijing are then compared with other cities to explore the differences in NO_x emissions. Subsequently, we evaluate emission inventories and satellite inversions against measured NO_x fluxes. In the end, the influences of NO_x emissions on O_3 flux are explored.

2. Experimental Section

2.1. Measurement site

Flux measurements were made during May to June 2023 on the meteorological tower at the Institute of Atmospheric Physics, Chinese Academy of Sciences (IAP, CAS) (39°58′28″ N, 116°22′16″ E) (Fig. 1). This site located between the third and the fourth ring roads of Beijing and is surrounded by parks, residential, commercial facilities, and busy roads. For the requirements of measurement height above the inertial sublayer and below boundary layer height for eddy covariance flux

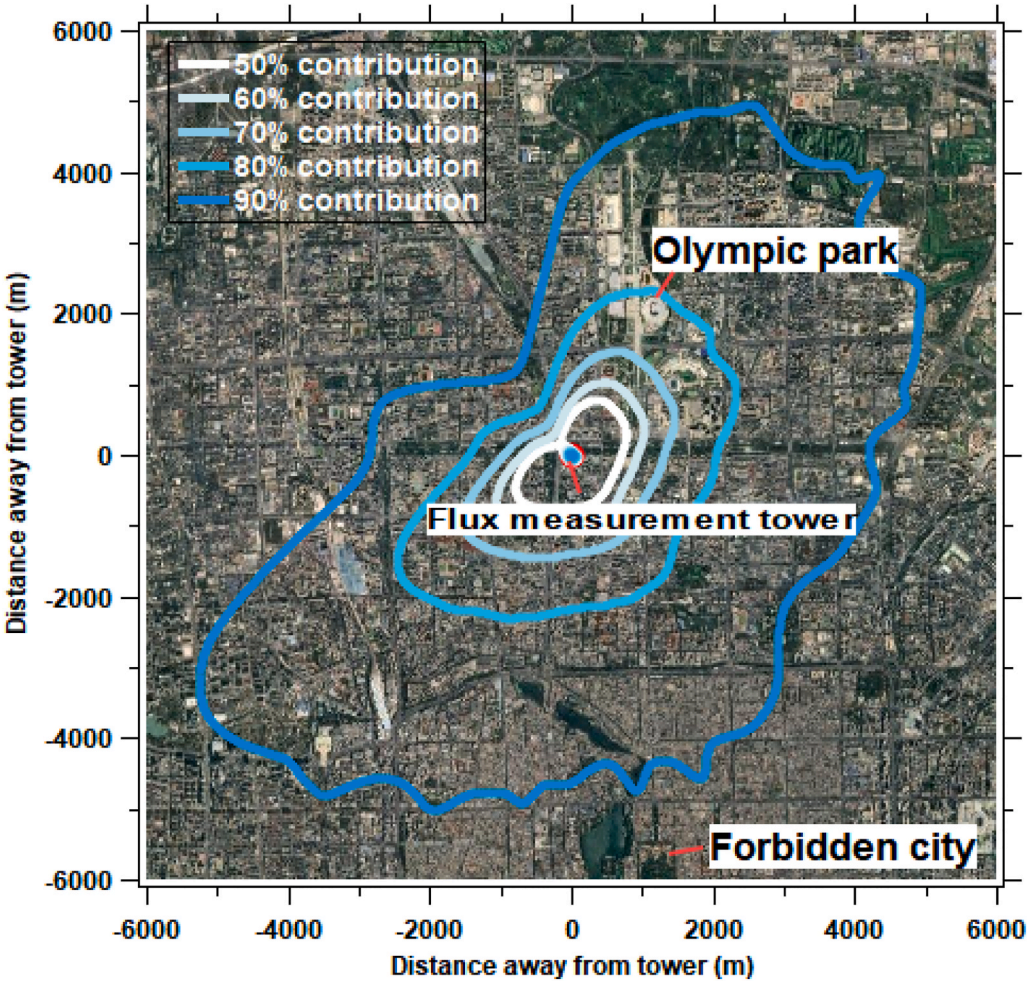


Fig. 1. Measurement site position and footprint of flux measurement during the measurement period. The lines represent the area contributing 50 %–90 % to the total flux, respectively.

(Foken, 2008; Matthews and Schume, 2022; Oke, 2017), the sampling inlet was placed at the 102 m platform of the tower. Previous flux measurements at this meteorological tower used the platform at this height as well (Acton et al., 2020; Huangfu et al., 2024; Squires et al., 2020).

2.2. Instrumentation

At the 102 m platform, the Integrated Open-Path Gas Analyzer 3D Sonic Anemometer (IRGASON) system (Campbell Scientific, Inc., USA) was used to measure wind speed and direction, CO_2 and H_2O mixing ratios at 10 Hz. Meanwhile, a 10 Hz chemiluminescence ozone instrument (FOS-SENSOR, Sextant Technology Ltd.) and a 1 Hz ultraviolet photometry ozone analyzer (model 205, 2B Tech, USA) were co-deployed for O_3 flux measurements on the tower, with the latter correcting FOS-SENSOR signal attenuation caused by coumarin reagent depletion (see Fig. S1 for methodology). The background measurement for the 2B 205 is conducted at a regularly intervals. Its detection limit and uncertainty are 2 ppbv (2σ, 10s) and 2 %, respectively. Cross-validation with other instruments has confirmed that the 10Hz O_3 concentrations measured by our method are accurate (Fig. S7).

In the tower base ground laboratory, we deployed two types of 1 Hz-capable NO_2 analyzers to measure NO_x and O_x fluxes respectively: a cavity attenuated phase shift analyzer (CAPS, Aerodyne Research, Inc.) measuring NO_x ($NO + NO_2$) via titration with excessive O_3, and a broadband cavity enhanced spectrometer NO_2 analyzer (BBCES) measuring O_x through NO titration (Fig. S2). CAPS and BBCES background measurements occurred at 30-min and 3-h intervals, respectively. Additionally, both CAPS and BBCES are regularly calibrated against certified commercial NO_2 cylinders under varying operational conditions to ensure data reliability (Fig. S4). Their detection limits are <0.2 ppbv (2σ, 1 s) for CAPS and 0.05 ppbv (1σ, 5 s) for BBCES, with corresponding uncertainties of 5 % and 4 %, respectively. Cross-validation with other instruments confirms the accuracy of the titration-based NO_x and O_x measurements (Fig. S7). Detailed instrument measurement, data correction, quality assurance and quality control for NO_x, O_3, O_x, and related species (including NO/NO_x, CH_4, VOCs) are provided in *Supplementary Information Section S1*.

2.3. Flux calculation and footprint analysis

The fluxes of NO_x, O_3, and O_x can be obtained from the covariance between the vertical wind speed and concentrations of various species according to the theory of eddy covariance (EC) method (Equation (1)).

$$F = \overline{w'C'} \quad (1)$$

where w' is instantaneous deviations of vertical wind speed ($w' = w - \overline{w}$, where $\overline{w}$ denote averages), and C' is instantaneous deviations of concentration ($C' = C - \overline{C}$). The flux was calculated over a 30 min averaging period. Detailed descriptions for lag-time determination, quality control, spectral analysis, storage flux correction and data comparisons can be found in *Supporting Information* (Figs. S5–8).

Footprint for flux measurements was determined by a two-dimensional parameterization footprint model (Kljun et al., 2015) for each 30 min flux period at 10-m-resolution (Supporting *Information Section S3*). This model is widely used in footprint modeling (Acton et al., 2020; Huangfu et al., 2024; Squires et al., 2020). Fig. 1 shows flux measurements represent average fluxes within ~75 km^2 of the site, where the footprint accounts for 90 % flux contribution.

2.4. Emissions data from satellite inversion and emission inventory

Measured NO_x fluxes are compared with emission estimates in various emission inventories. The Chinese Multi-Resolution Emission Inventory (MEIC) are available at 0.01°, 0.1° and 0.25° resolution for 2017, and at 0.25° resolution for 2020 (Geng et al., 2024; Zheng et al., 2018). In addition, the comprehensive global emission inventory for greenhouse gases and air pollutants (PKU v1) (Huang et al., 2017; Lin et al., 2023), and the Emissions Database for Global Atmospheric Research (EDGAR v8.1) (Crippa et al., 2024) were also compared with NO_x fluxes measured in this study. Footprint-matching emissions were calculated by downscaling gridded inventories to 10-m-resolution and area-averaging within the flux footprint.

Here, eddy covariance flux measurements were also compared against two satellite inversions: 1) TROPOMI-based 5-km-resolution NO_2 emissions across China during summer 2022 using an updated retrieval method of Kong et al. (2022). The satellite data in Kong et al. (2022) were derived from the POMINO-TROPOMI product (Liu et al., 2020), which accounts for aerosol and surface reflectivity effects relative to the official product (TM5-MP-DOMINO OFFLINE v1.1.0) (Geffen et al., 2019). Here, TROPOMI-based NO_2 emissions data were processed similarly to those for emission inventories. 2) Geostationary Environmental Monitoring Spectrometer (GEMS) derived hourly NO_2 emissions for East Asian cities (including Beijing) for the summer of 2021 (Xu et al., 2023). During inversion process, the GEMS NO_2 v1.0 product was utilized (KESC, 2021), with filtered using criteria of effective cloud fraction and solar zenith angle (Kim et al., 2023). The average emission flux for urban Beijing is determined by the whole city emission divided by urban build-up area (1469 km^2).

3. Results and discussion

3.1. Overview of the NO_x, O_3 and O_x fluxes

Fig. 2 presents a synthesis of NO_x, O_3, and O_x fluxes along with traffic index data collected during this campaign. The 24-h average NO_x concentration measured during the study period was 14.6 ± 12.7 ppbv (Fig. S9). As anticipated, NO_x exhibited predominantly upward fluxes (91.7 % flux data) throughout the campaign. Diurnal flux values ranged from −20.8 to 66.2 nmol/m^2/s, with a 24-h average flux of 10.4 ± 10.7 nmol/m^2/s. The fluxes measured in 2023 were 44 % lower than NO_x flux (19.3 ± 10.4 nmol/m^2/s) measured at the same site in 2017 (Squires et al., 2020), similar to 57 % reduction of NO_x concentrations during the two campaigns. The decline of NO_x concentrations in Beijing is also confirmed by routine measurement (in terms of NO_2) from China National Environmental Monitoring Center (CNEMC, 2023) (Fig. S10).

Analysis of diurnal profile of NO_x flux revealed relatively stable emissions between 10:00–16:00, followed by a pronounced afternoon peak (18:00). This pattern aligns with established relationships between NO_x emissions and traffic flow (Drysdale et al., 2022; Karl et al., 2017). To investigate traffic-related emission variations, we conducted a weekday-weekend comparison. Fig. 3a-b demonstrates strong temporal coincidence between NO_x flux peaks and traffic indices during weekdays (18:00). In contrast, weekend observations showed no notable consistency between traffic index and NO_x emissions. This discrepancy likely stems from distinct travel patterns (destinations and routes) between weekdays and weekends. Specifically, weekend congestion areas may exhibit greater spatial dispersion compared to weekdays, causing vehicle emissions to frequently occur outside the footprint. Consequently, weekend evening traffic peak fail to align with NOx flux peak. Comparative analyses indicate that traffic index and NO_x emissions are 10 % and 14 % lower on weekends than on weekdays, respectively. While atmospheric temperature is recognized to influence non-transport NO_x sources (e.g., soil emissions and power generation) under hot conditions (Zhu et al., 2023), our measurements showed negligible temperature dependence in both NO_x concentrations and fluxes (Fig. 3c–d).

Moreover, moderate correlations between NO_x and two aromatics benzene (R = 0.47) and toluene (R = 0.52) were observed during 17:00 to 20:00 (Fig. 4a–b), indicating common source contributing to emissions of NO_x and aromatics, most likely combustion sources, e.g.,

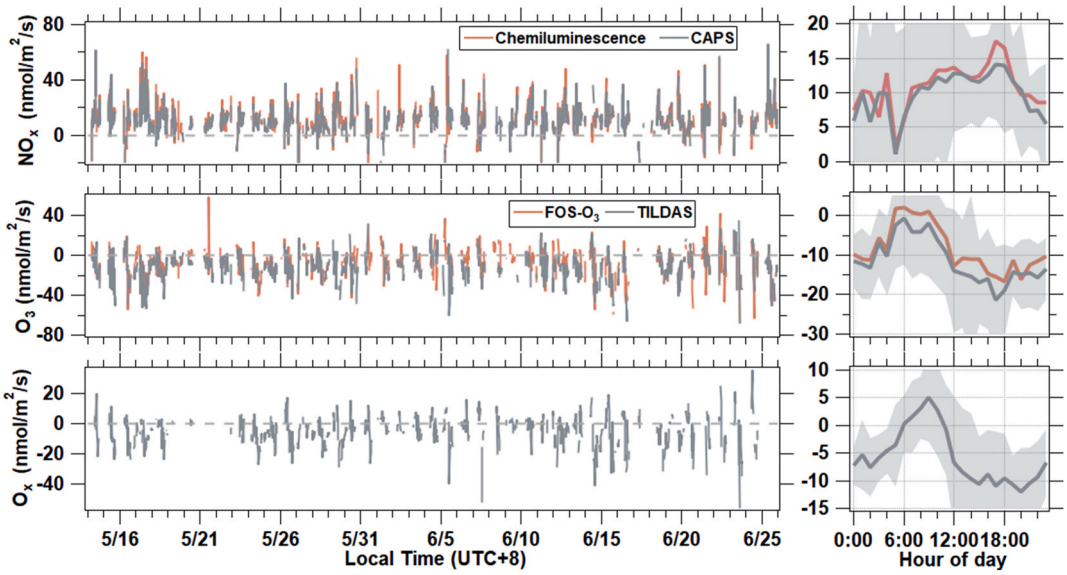


Fig. 2. Time series (left panel) and diurnal profiles (right panel) of measured NO_x, O_3 and O_x fluxes.

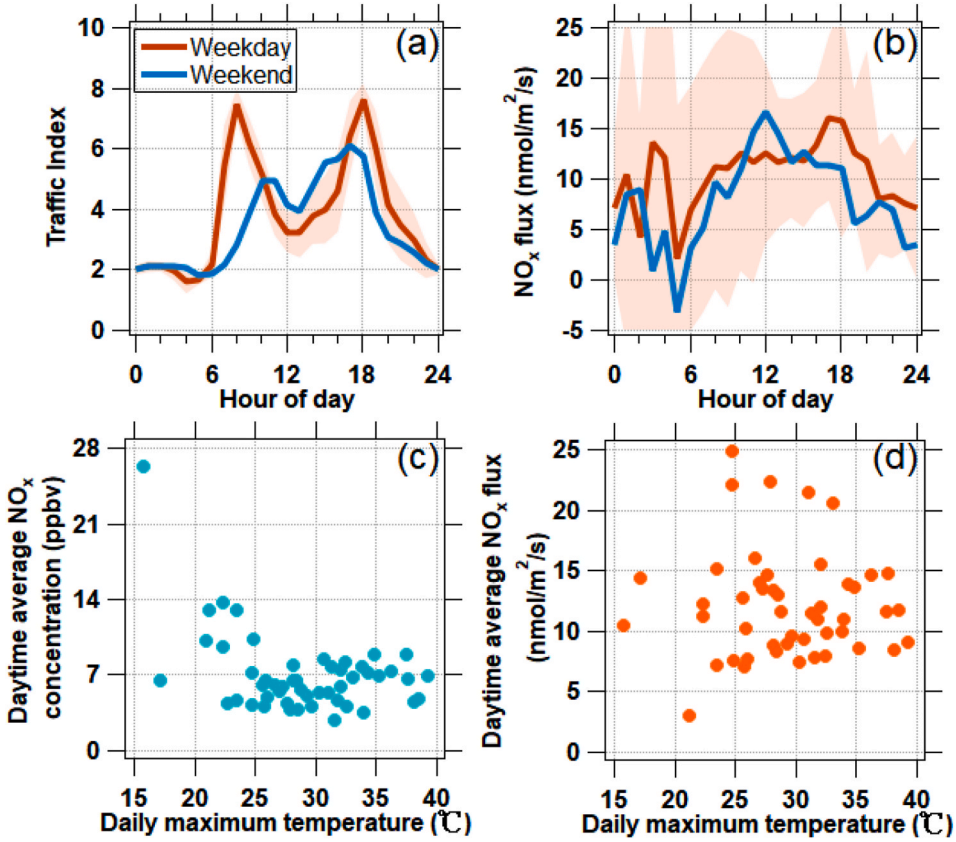


Fig. 3. The weekend-weekday effects of traffic index (a) and NO_x flux (b), and temperature dependence of NO_x concentration (c) and flux (d). The traffic index data is sourced from Beijing Transport Institute (BTI, 2023).

vehicles or residential combustion (Shaw et al., 2015; Yang et al., 2018b). Residential combustion of natural gas, especially during cooking and heating (Cliff et al., 2025; Lebel et al., 2022), may contribute significantly to urban NO_x emissions. However, poor correlations emerged between NO_x fluxes and both CH_4 ($R = 0.27$) and cooking tracer nonanal (Coggon et al., 2024; Klein et al., 2016) fluxes ($R = 0.20$) during 17:00 to 20:00 (Fig. 4c–d), indicating potentially small contributions to NO_x from natural gas usage during summer in Beijing. Collectively, these findings suggest vehicular emissions as the primary contributor to urban NO_x emissions in summer Beijing.

NO and NO_2 fluxes were individually measured using the chemiluminescence NO_x analyzer. Analysis of the data reveals that 85–97 % of daytime NO_x emissions were measured in the form of NO_2, with the NO_2/NO_x flux ratio exhibiting a distinct diurnal increase (Fig. S11a). This pattern is consistent with the titration effect caused by elevated O_3 concentrations and enhanced downward fluxes during daylight hours.

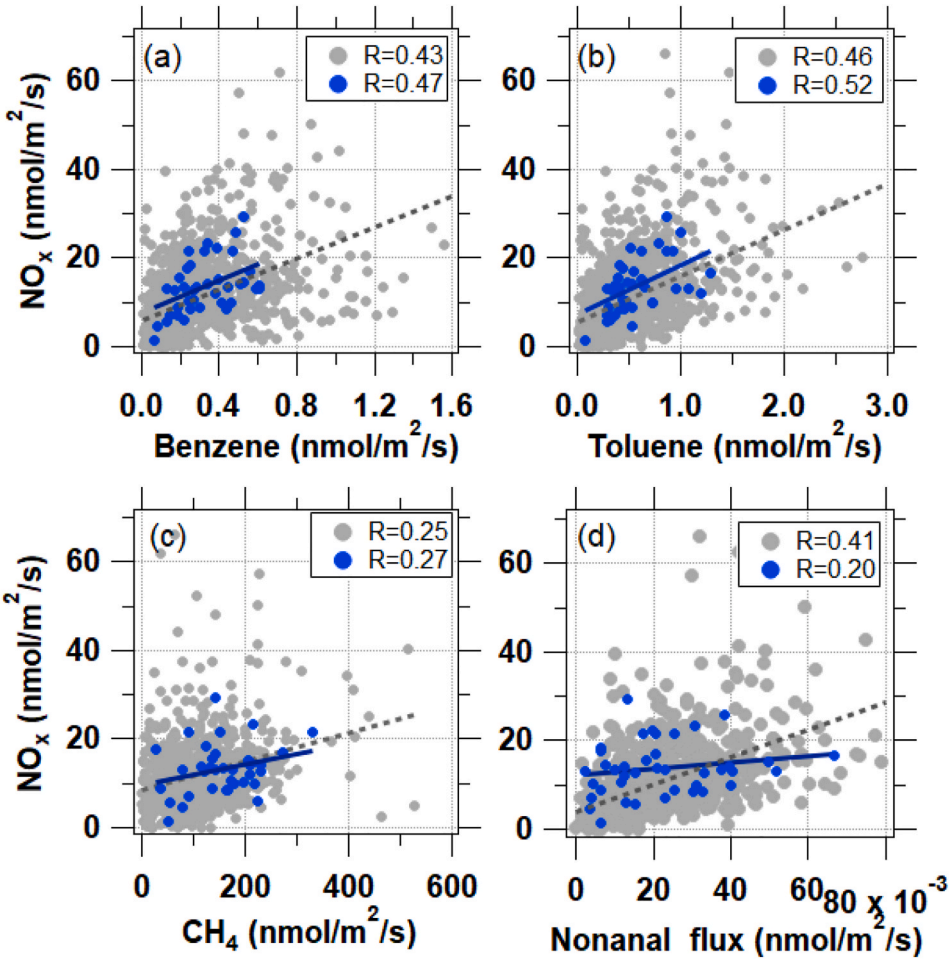


Fig. 4. Scatter plots of NO_x flux with benzene (a), toluene (b), CH_4 (c), nonanal (d) fluxes, respectively. The gray dots represent each half-an-hour measurement, while blue dots denote the average values between 17:00 and 20:00 for each day. (For interpretation of the references to color in this figure legend, the reader is referred to the Web version of this article.)

The ratios of NO_2/NO_x flux remain elevated under conditions of low O_3 concentrations (<20 ppbv) (Fig. S11b). However, this observation does not unequivocally indicate a dominant emissions in terms of NO_2, as demonstrated by that fast NO-to-NO_2 conversion by O_3 remains important even under low atmospheric concentrations of O_3 (Karl et al., 2023). This poses a significant challenge for quantifying direct NO_2 emissions in urban environments.

O_3 fluxes exhibited dominant downward tendencies with a mean of -10.8 ± 13.7 nmol/m^2/s, accompanied by a mean concentration of 53.6 ± 29.7 ppbv (Fig. 2 and Fig. S9). Diurnally, O_3 flux exhibited an absolute minimum around midday to early afternoon. During the early morning period (05:00–10:00), the O_3 flux approached zero. Karl et al. (2023) emphasize that O_x fluxes provide more reliable indicators of actual depositional O_3 fluxes near urban surfaces as the result of NO-O_3 photochemical reactions. This highlights the importance of O_x flux measurements for characterizing atmospheric oxidation. Consistent with O_3 behavior, O_x fluxes demonstrated substantially downward fluxes with a 24-h average of -4.8 ± 9.9 nmol/m^2/s, corresponding to a 24-h average concentration of 79.6 ± 30.0 ppbv (Fig. 2 and Fig. S9). Using O_x flux as the more reliable parameter, we determined that the average ozone deposition velocity (V_d) is 0.24 ± 0.25 cm/s ($V_d = |O_x$ *flux/O_3 concentration*|), which is significantly lower than the value determined using ozone flux (0.62 ± 0.50 cm/s). This implies the large influences of NO_x titration effect on ozone flux in urban regions.

3.2. *Drivers of NO_x emission disparities among cities*

Concentrations and fluxes of NO_x measured in this work are compared with measurements in other cities, including London in UK (Cliff et al., 2025; Drysdale et al., 2022; Lee et al., 2015; Vaughan et al., 2016), Innsbruck in Austria (Karl et al., 2023; Karl et al., 2017), Los Angeles in U.S. (Nussbaumer et al., 2023), and San Joaquin Valley in U. S. (Zhu et al., 2023) (Fig. 5a–b). Similar diurnal profiles of both NO_x concentrations and fluxes are observed in different cities. NO_x concentrations usually show the highest concentrations in the morning and a second smaller peak in the evening, with the minimum concentrations in the early afternoon. Different to NO_x concentrations, NO_x fluxes demonstrated the strongest emission fluxes during the daytime, with marked lower emissions at night, suggesting common controls of human activities on NO_x emissions in various cities.

We generally observe similar concentration ranges for NO_x in different cities, with apparently higher concentrations measured in 2017 in Beijing than other observations. With the substantially decrease of NO_x concentrations in recent years, NO_x concentrations observed in Beijing in 2023 are comparable to other cities. While NO_x concentrations showed spatial consistency across cities, NO_x fluxes exhibited notable regional differences. The measured NO_x fluxes in Beijing in 2023 are comparable to observations in Los Angeles, San Joaquin Valley, and Innsbruck (Cliff et al., 2025; Karl et al., 2023; Zhu et al., 2023). London exhibited substantially higher flux than other cities (Fig. 5c). Emissions of diesel vehicle have been identified as a major contributor to urban

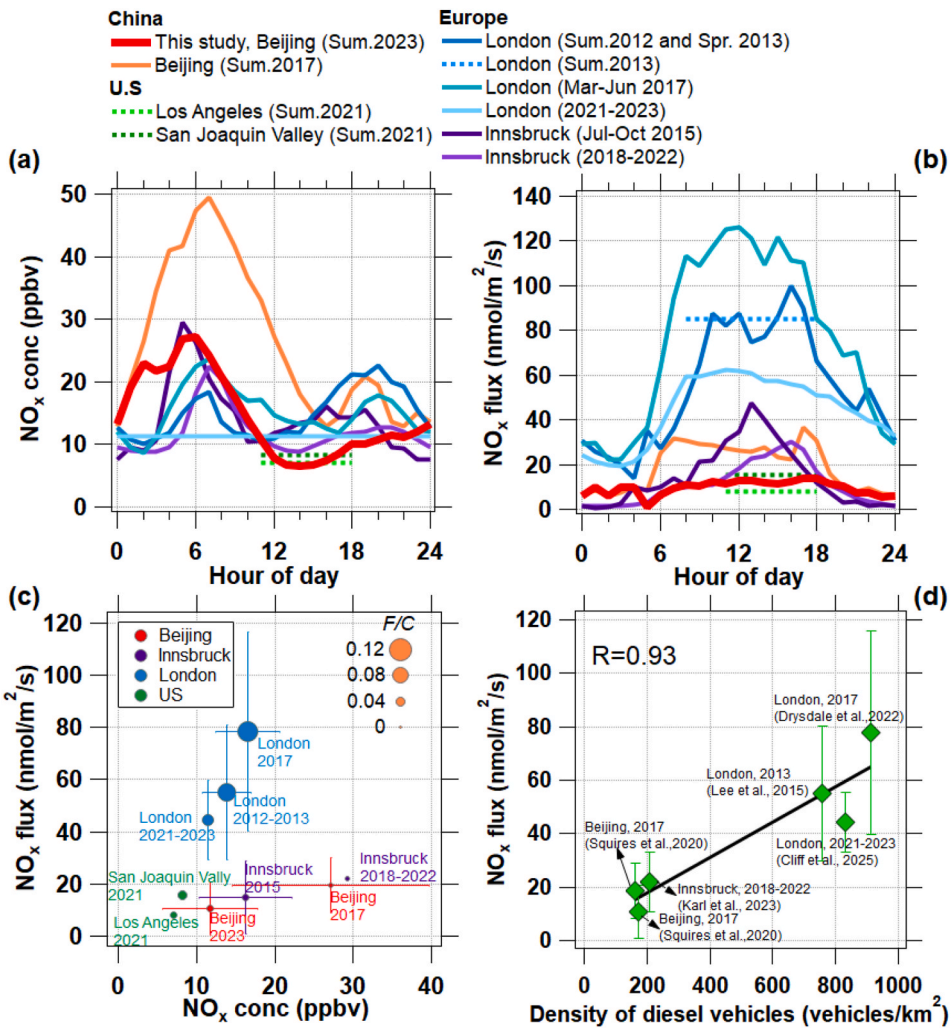


Fig. 5. Comparison of diurnal profiles of NO_x concentrations (a) and fluxes (b) measured in Beijing by this study and also in 2017 (Squires et al., 2020), Los Angeles (Nussbaumer et al., 2023), San Joaquin Valley (Zhu et al., 2023), London (Cliff et al., 2025; Drysdale et al., 2022; Lee et al., 2015; Vaughan et al., 2016) and Innsbruck (Karl et al., 2023; Karl et al., 2017). The green and blue dashed lines represent results from airborne flux measurements. (c) The average NO_x flux versus concentration for different cities. The data points are sized using the ratio of flux/concentration (*F/C*) of NO_x. The 2021–2023 annual average NO_x concentrations in London were sourced from the UK Environment Agency (UK Environmental Agency, 2024). (d) Scatter plot of NO_x flux versus diesel vehicle density. When conversion between different flux units (mass units and molar), the molecular mass of NO (30 g/mol) was used. (For interpretation of the references to color in this figure legend, the reader is referred to the Web version of this article.)

NO_x pollution (Breuer et al., 2020; Burgard et al., 2006; Yang et al., 2018a). Regional variations in diesel vehicle densities significantly explain the observed intercity differences in NO_x fluxes. Fig. 5d demonstrates a positive correlation between diesel vehicle density and NO_x flux across cities (R = 0.93). In recent years, Beijing has achieved significant reductions of NO_x emissions despite a marginal increase in diesel vehicle fleet (especially heavy trucks) (NBSC, 2024), as shown in Fig. 5d. This success stems from but the significant improvements in vehicle technology (Ai et al., 2022). London exhibits a notably high average diesel vehicle density of 830 vehicle/km^2, 4–5 times higher than Beijing and Innsbruck. Diesel vehicle density in the UK steadily increased before 2019 (DTDVLA, 2023). Concurrently, NO_x fluxes measured at the BT Tower in 2017 showed a 42 % increase compared to 2013 measurements from the same site (Fig. 5c), whereas NO_x emissions measured in 2021–2023 were 44 % lower than those in 2017, as the result of reduction of vehicular emissions (Cliff et al., 2025).

From the perspective of diurnal profile (Fig. 5b), Beijing exhibits obvious NO_x emissions in the early morning in addition to daytime emissions, a phenomenon not observed in London or Innsbruck. As shown in Fig. 6, by analyzing early morning (00:00–06:00) to daytime (11:00–18:00) ratio of NO_x flux, we obtain the ratio in Beijing as 0.59 ± 0.22, which is 1.8–2.8 times of those in London (0.32 ± 0.06) and Innsbruck (0.21 ± 0.05). Using four days with minimal storage term ($Flux_{storage}/Flux_{EC}$ ratio <0.3) derives slightly lower ratio (0.51 ± 0.23), which is still notably higher than London and Innsbruck. These differences stem from a unique air quality policy implemented in Beijing, which only allows entry of heavy-duty trucks to urban core region during night hours (23:00–06:00) (BTMB, 2009), to reduce diesel usage as 80 % of China's heavy-duty truck fleet use diesel (Mao et al., 2025). Consequently, this policy would shift NO_x emissions toward early morning, which enhances the early morning to daytime ratio.

3.3. Comparison with emission inventories and satellite inversion

NO_x emissions quantified by eddy covariance method serve as a critical benchmark for validating emission inventories. Within the footprint area, we perform comparisons between measured NO_x fluxes and three NO_x inventory products (Fig. 7). For these emission inventories, we find that agriculture, power plants and industrial sectors account for 34–46 % (MEIC), 57 % (PKU), and 57 % (EDGAR) of

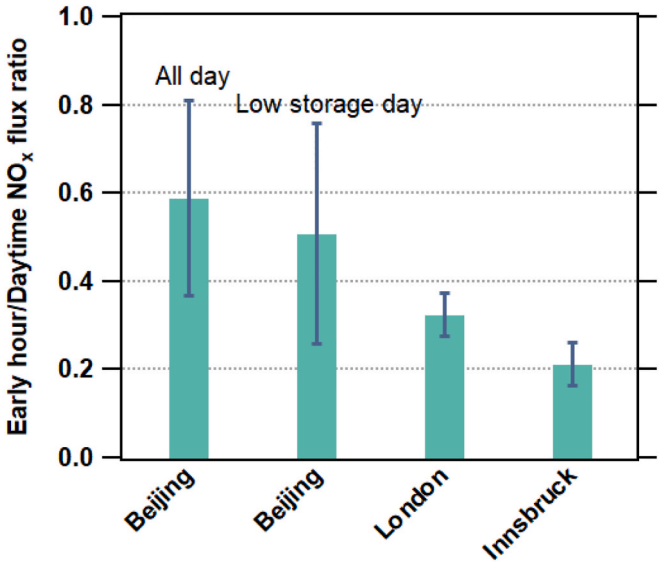


Fig. 6. Ratio of NO_x fluxes between the early morning (00:00–06:00) and daytime (11:00–18:00) in different cities.

estimated NO_x emissions (Fig. S12). To our knowledge, these source sectors are not present in the measurement footprint, which suggests that these sectors may be incorrectly allocated to footprint area. Therefore, we will only focus on comparisons of transportation and residential sectors with flux measurements.

Emission inventories indicate significant variations for emission intensity within the footprint area (Fig. S13), which could introduce significant uncertainty from spatial alignment in comparison with fluxes. Here, the uncertainties from the spatial alignment are determined from the change of NO_x emissions from each emission inventory using footprint areas at 50 %–90 % of flux contribution (Fig. 7c), which exhibit fluctuations in the range of 30 %–62 % for different emission inventories. It suggests that the uncertainty introduced by spatial alignment can be as large as 60 %. Considering the uncertainty from flux measurements (20 %), the combined uncertainty for comparison would propagate to be 70 %.

With the estimated uncertainty, we will discuss the comparison of flux measurements with emission inventory using the footprint area at 90 % of flux contribution (Fig. 7a). The MEIC products with 0.1° and 0.25° in both 2017 and 2020 showed similar NO_x emission estimates, which are 2.7–4.5 times of NO_x fluxes measured in 2023, respectively. Considered the year differences between flux measurements and inventory estimates, MEIC estimate for 2017 is still higher than flux measurements in summer of 2017 by 156 %, as discussed in details in

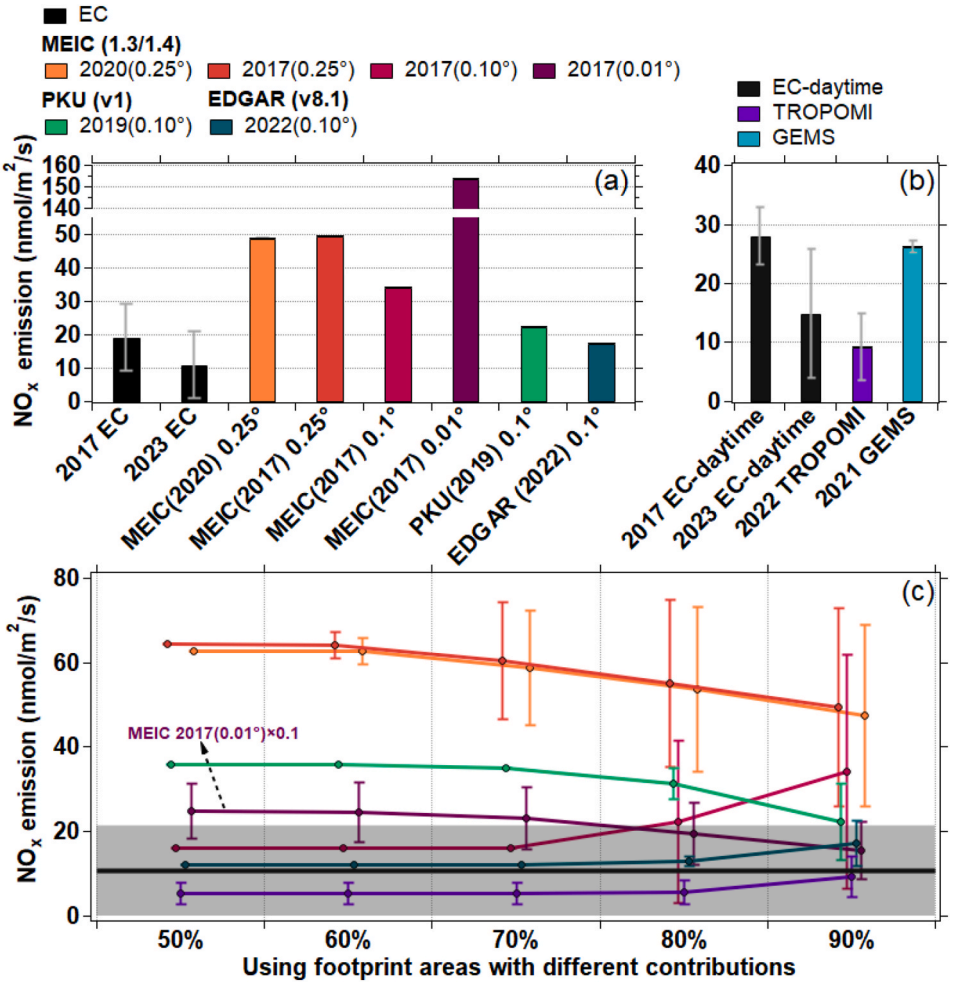


Fig. 7. (a) Comparison of eddy covariance (EC) NO_x flux with emission inventories including MEIC (Geng et al., 2024; Zheng et al., 2018), PKU (Huang et al., 2017; Lin et al., 2023), and EDGAR (Crippa et al., 2024) using footprint at 90 % of flux contribution. (b) Comparison of daytime (11:00–18:00) EC NO_x flux with NO_x emissions derived from inversion of satellite measurements (TROPOMI and GEMS) (Kong et al., 2022; Xu et al., 2023) using footprint at 90 % of flux contribution. (c) Estimated NO_x emissions from emission inventories and satellite retrievals using footprint at different percentage of flux contribution. The black line and gray band represent average and standard deviation of flux measurement in 2023. Note that the results from MEIC 2017 at 0.01° resolution is multiples by 0.1 for sake of clarity.

(Squires et al., 2020). Similarly, NO_x emission in PKU inventory is 2.1 time of flux observations in 2023. These differences between flux measurements and emission inventory are clearly higher than 70 % of uncertainty in comparison. As NO_x emission in winter is only 20 % higher than summer (Squires et al., 2020), seasonal variations could not explain the difference between flux measurements and emission inventory (estimated for a whole year). The high-resolution version (0.01°) of MEIC determines considerably higher NO_x emissions than other lower-spatial resolution products. As a novel spatial allocation method is used in the high-resolution 0.01° MEIC inventory, this result indicates that the allocation method may fail to correctly assign NO_x emissions in terms of kilometer-scale fine resolution in urban regions. It is surprising that the EDGAR global inventory illustrates reasonable agreement with NO_x flux measurement with deviation only by 57 %. Previous studies showed that EDGAR emission inventory usually obtain slightly lower but comparable NO_x emissions for China (Li et al., 2017). We suspect the differences between EDGAR and other emission inventories may be caused by different proxies used for spatial allocation.

As MEIC emission inventory provides emission estimates in multiple different years, it also provides an opportunity to compare NO_x emissions changes between inventory and flux measurements. As discussed above, the concentration and flux of NO_x in Beijing decreased by 57 % and 44 % from 2017 to 2023, respectively (Fig. 4c). Contrastingly, MEIC estimated transportation sector emission (0.25°) decreased by only 2.8 % from 2017 to 2020, whereas residential emissions increased by 20 %. These differences imply that MEIC inventory may underestimate recently quick reduction of NO_x emissions in megacities like Beijing.

In addition to emission inventory, NO_x flux measurements are also compared to inversions from satellite retrievals. As satellite measurements only cover daytime, averages of NO_x flux between 11:00 and 18:00 are used for comparison (Fig. 7b). In contrast to emission inventory, we observe comparable estimates between flux measurements and inversion from satellite retrievals, considering combined uncertainties in the comparison, including footprint determination and potentially fine-scale spatial heterogeneity not resolved by both methods. Specifically, TROPOMI inversion in 2019 (Kong et al., 2022) 38 % lower and GEMS inversion in 2021 (Xu et al., 2023) 40 % higher than NO_x fluxes measured in 2023. However, if the yearly decline of NO_x emissions considered as inferred as NO_x flux differences in 2017 and 2023, GEMS inversion appears to be more comparable to flux measurements. This comparison indicate flux measurements could be used as a reference for validating satellite retrievals, as considerable uncertainties in satellite measurements and inversion processes from column concentrations to ground emissions also exist (Lorente et al., 2017; van Geffen et al., 2022; Verhoelst et al., 2021).

3.4. *Influence of NO_x on near-surface O_3 downward flux*

The Dahmköhler (Da) number, a dimensionless parameter quantifying the relative time scales of transport and chemical reaction rates (*Section S4 in Supplementary Information*), has been widely applied in atmospheric chemistry studies (Plake et al., 2015; Rinne et al., 2012; Vuolo et al., 2017). Our campaign measurements revealed an average Da number of 3.3 ± 2.6 for the NO-NO_2-O_3 reaction system, and average

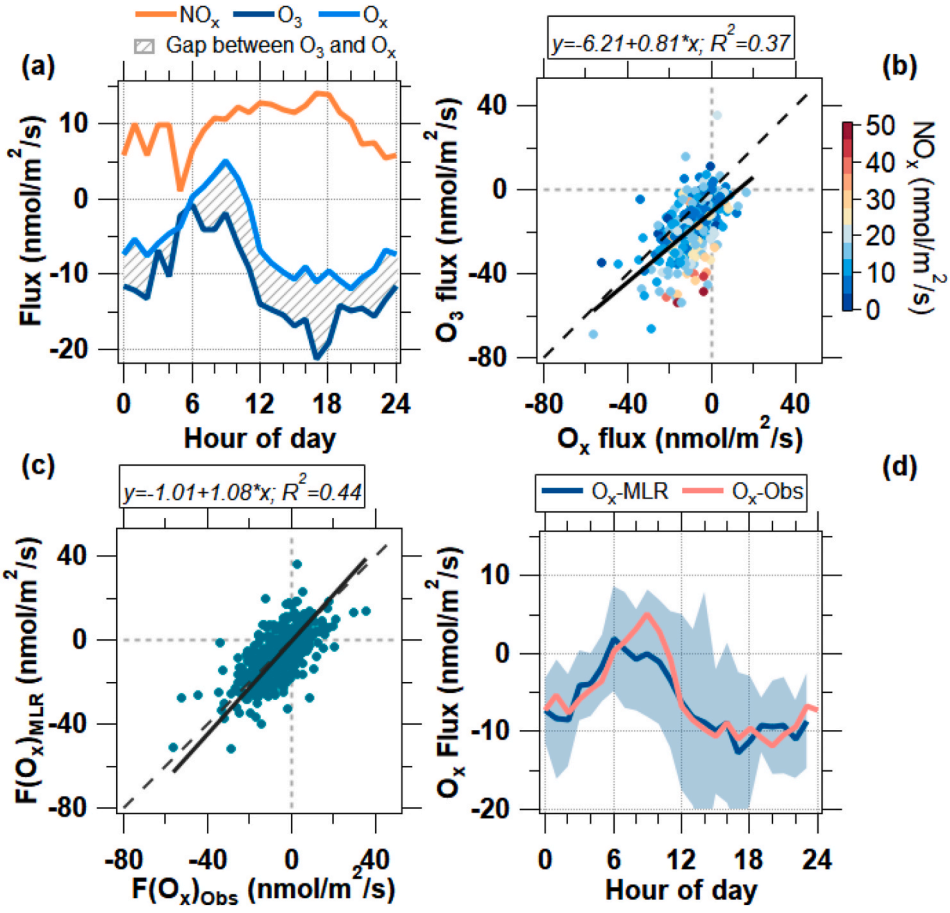


Fig. 8. (a) Diurnal variations of NO_x, O_3 and O_x fluxes, with the gray shaded as the difference between O_3 and O_x fluxes. (b) O_x versus O_3 fluxes in the daytime (11:00–19:00), color-coded by the NO_x flux. (c) Scatter plot of O_x flux from MLR versus observed O_x flux. The dashed black lines in (b) and (c) represent 1:1 line and the solid black lines represent the fits from the data points. (d) The diurnal profiles of O_x flux calculated from MLR and the observed O_x flux. (For interpretation of the references to color in this figure legend, the reader is referred to the Web version of this article.)

flux Da number for O_3 is 2.5 ± 10.4 (Fig. S14). These values indicate that O_3 concentration and flux in Beijing are strongly influenced by NO-to-NO_2 conversion processes. Fig. 8a demonstrates pronounced discrepancies between O_x and O_3 fluxes under elevated NO_x emission conditions. Analysis in Fig. 8b further illustrates O_x flux deviates increasingly from the 1:1 line with rising NO_x flux, suggesting the NO_x emissions significantly modulate surface flux of O_3, and O_x flux is a more accurate indicator of the describe depositional O_3 flux near-surface in urban environments.

Here, the influence of NO_x emissions on O_3 downward fluxes was quantified using a multiple linear regression (MLR) method (Equation (2)):

$$F_{O_x} = k_1 F_{O_3} + k_2 F_{NO_x} \quad (2)$$

where F_{O_x}, F_{O_3}, and F_{NO_x} represent the fluxes of O_x, O_3, and NO_x, respectively. Regression analysis yielded $k_1 = 0.88$ and $k_2 = 0.36$, with a moderate correlation coefficient ($R^2 = 0.44$) between modeled and observed O_x fluxes (Fig. 8c). Our results suggest that the MLR method can appropriately characterize the relationships among NO_x, O_3, and O_x fluxes (Fig. 8d). Discrepancies between predictions and measurements are particularly evident in the morning period (06:00–11:00) due to storage term influence (Fig. 8d), prompting us to focus on daytime (11:00–18:00) when titration effects dominate. The titration effect for NO_x emissions on O_3 downward flux is determined from the ratio of $|k_2 F_{NO_x} / k_1 F_{O_3}|$, obtaining an average of 54 ± 53 %. Such a pronounced titration effect necessitates prioritizing the analysis of O_x flux over O_3 flux.

4. Conclusions

In this study, we simultaneously conducted flux measurements of NO_x, O_3 and O_x at the Beijing Meteorological Tower from May to June 2023. The observed NO_x fluxes exhibited a net upward trend, indicating persistent NO_x emissions in Beijing. Notably, these 2023 NO_x flux and concentrations showed approximately 50 % reduction compared to 2017 measurements at the same site. Statistical analysis of NO_x flux variability revealed a strong consistency with traffic flow in Beijing, particularly diesel vehicle fleet. However, NO_x emissions estimated in emission inventories show overestimation than flux measurements, indicating that the inventories may fail to accurately estimate NO_x emissions in urban scale. A further comparison with satellite retrieval obtained reasonable agreement.

By comparing reaction time scales of NO_x photochemistry and atmospheric transport, we demonstrate that O_3 downward fluxes are significantly influenced by NO-to-NO_2 conversion processes. To quantify the influence of NO_x emission on O_3 flux, we applied a multiple linear regression method to describe the relationship between NO_x, O_3, and O_x fluxes. NO_x-induced titration effect reduces surface O_3 deposition fluxes by 54 ± 53 %. These results support that the flux measurement of O_x should be conducted and used in urban regions to represent the deposition flux of O_3, rather than direct O_3 flux.

As the policy implementation intensifies, NO_x emissions are expected to constantly decline, which will reduce their impact on the O_3 downward flux. Our results along with others (Cliff et al., 2025; Karl et al., 2023) demonstrate that flux measurements in urban regions could track this reduction path to provide quantitively constraints on these changes and offer the opportunity to validate the estimate from other methods, including emission inventory and satellite retrievals.

CRediT authorship contribution statement

Xiaoxiao Zhang: Writing – original draft, Visualization, Validation, Investigation, Formal analysis, Data curation. **Bin Yuan:** Writing – review & editing, Resources, Project administration, Funding acquisition, Formal analysis, Conceptualization. **Yibo Huangfu:** Writing – review & editing, Software, Data curation. **Huizhi Liu:** Supervision, Resources, Project administration. **Thomas Karl:** Writing – review & editing, Methodology. **Ming Chang:** Data curation. **Shiyi Chen:** Data curation. **Tao Song:** Resources. **Jintai Lin:** Writing – review & editing, Investigation. **Guannan Geng:** Data curation. **Hongjuan Li:** Data curation. **Eran Tas:** Resources, Funding acquisition.

Declaration of competing interest

The authors declare that they have no known competing financial interests or personal relationships that could have appeared to influence the work reported in this paper.

Acknowledgment

This work was supported by the National Natural Science Foundation of China (grant No. 42121004, 42275103, 42230701, 42205094, 42161144010), National Key Research and Development Program of China (grant No. 2023YFC3710900, 2023YFC3706103, 2023YFC3706200), Guangdong Basic and Applied Basic Research Foundation (Grant No. 2025A1515011156). We acknowledge Ziyang Liu, Xianjun He, Yihua Sun, and Yuanting Zhang at Jinan University for their contributions to the experimental work and data analysis. We also extend our sincere appreciation to Dr. Shengrong Lou, Dr. Yang Liu, Mr. Xiaodong Chen, and Professor Min Shao for their invaluable contributions and support to this research.

Appendix A. Supplementary data

Supplementary data to this article can be found online at https://doi.org/10.1016/j.envpol.2025.127213.

Data availability

Data will be made available on request.

References

Acton, W.J.F., Huang, Z., Davison, B., Drysdale, W.S., Fu, P., Hollaway, M., Langford, B., Lee, J., Liu, Y., Metzger, S., Mullinger, N., Nemitz, E., Reeves, C.E., Squires, F.A., Vaughan, A.R., Wang, X., Wang, Z., Wild, O., Zhang, Q., Zhang, Y., Hewitt, C.N., 2020. Surface-atmosphere fluxes of volatile organic compounds in Beijing. Atmos. Chem. Phys. 20, 15101–15125.

Ai, Y., Cui, Y., Ge, Y., Wu, X., Wu, T., Liu, X., Shen, Y., Liu, M., Wan, Y., Yi, H., Xue, Y., 2022. Study on the control targets and measures for total diesel consumption from mobile sources in Beijing, China. Front. Environ. Sci. 10, 1068861.

Beijing Traffic Management Bureau (BTMB), 2009. Announcement by the Beijing Municipal Public Security Bureau regarding adjustments to route restrictions for non-local cargo vehicles entering Beijing. https://jtgl.beijing.gov.cn/jgj/jgxx/gsgg/jttg/bjsgajtg/335154/index.html.

Beijing Transport Institute (BTI), 2023. Traffic Index of Beijing. Last. https://www.bjtrc.org.cn/Public/index.html.

Breuer, J.L., Samsun, R.C., Peters, R., Stolten, D., 2020. The impact of diesel vehicles on NOx and PM10 emissions from road transport in urban morphological zones: a case study in North Rhine-Westphalia, Germany. Sci. Total Environ. 727, 138583.

Burgard, D.A., Dalton, T.R., Bishop, G.A., Starkey, J.R., Stedman, D.H., 2006. Nitrogen dioxide, sulfur dioxide, and ammonia detector for remote sensing of vehicle emissions. Rev. Sci. Instrum. 77, 014101.

China National Environmental Monitoring Centre (CNEMC), 2023. Real-time China urban air quality release platform. Last. https://air.cnemc.cn:18007/.

Cliff, S.J., Drysdale, W., Lewis, A.C., Møller, S.J., Helfter, C., Metzger, S., Liddard, R., Nemitz, E., Barlow, J.F., Lee, J.D., 2025. Evidence of heating-dominated urban NOx emissions. Environ. Sci. Technol. 59, 4399–4408.

Coggon, M.M., Stockwell, C.E., Xu, L., Peischl, J., Gilman, J.B., Lamplugh, A., Bowman, H.J., Aikin, K., Harkins, C., Zhu, Q., Schwantes, R.H., He, J., Li, M., Seltzer, K., McDonald, B., Warneke, C., 2024. Contribution of cooking emissions to the urban volatile organic compounds in Las Vegas, NV. Atmos. Chem. Phys. 24, 4289–4304.

Crippa, M., Guizzardi, D., Pagani, F., Schiavina, M., Melchiorri, M., Pisoni, E., Graziosi, F., Muntean, M., Maes, J., Dijkstra, L., Van Damme, M., Clarisse, L., Coheur, P., 2024. Insights into the spatial distribution of global, national, and subnational greenhouse gas emissions in the Emissions Database for Global Atmospheric Research (EDGAR v8.0). Earth Syst. Sci. Data 16, 2811–2830.

de Vries, W., 2021. Impacts of nitrogen emissions on ecosystems and human health: a mini review. Curr. Opin. Environ. Sci. Health. 21, 100249.
Department for Transport and Driver and Vehicle Licensing Agency (DTDVLA), 2023. Accredited official statistics status of vehicle licensing statistics. Last. https://www.gov.uk/government/publications/vehicles-statistics-guidance/national-statistics-status-of-vehicle-licensing-statistics.
Desjardins, R.L., Worth, D.E., Pattey, E., VanderZaag, A., Srinivasan, R., Mauder, M., Worthy, D., Sweeney, C., Metzger, S., 2018. The challenge of reconciling bottom-up agricultural methane emissions inventories with top-down measurements. Agric. For. Meteorol. 248, 48–59.
Drysdale, W.S., Vaughan, A.R., Squires, F.A., Cliff, S.J., Metzger, S., Durden, D., Pingintha-Durden, N., Helfter, C., Nemitz, E., Grimmond, C.S.B., Barlow, J., Beevers, S., Stewart, G., Dajnak, D., Purvis, R.M., Lee, J.D., 2022. Eddy covariance measurements highlight sources of nitrogen oxide emissions missing from inventories for central London. Atmos. Chem. Phys. 22, 9413–9433.
Foken, T., 2008. Micrometeorology. Springer, Berlin.
Geffen, J.H.G.M.v., Eskes, H.J., Boersma, K.F., Veefkind, J.P., Maasakkers, J.D., 2019. TROPOMI ATBD of the total and tropospheric NO2 data products; Royal Netherlands Meteorological Institute, Ministry of infrastructure and water management. https://sentiwiki.copernicus.eu/_attachments/1673595/S5P-KNMI-L2-0005-RP%20-%20Sentinel-5P%20TROPOMI%20ATBD%20NO2%20data%20products%202024%20-%202.8.0.pdf?inst-v=e9b0dc9b-a734-4403-9001-41ebb5a2cae9.
Geng, G., Liu, Y., Liu, Y., Liu, S., Cheng, J., Yan, L., Wu, N., Hu, H., Tong, D., Zheng, B., Yin, Z., He, K., Zhang, Q., 2024. Efficacy of China's clean air actions to tackle PM2.5 pollution between 2013 and 2020. Nat. Geosci. 17, 987–994.
Handisides, G.M., Plaß-Dülmer, C., Gilge, S., Bingemer, H., Berresheim, H., 2003. Hohenpeissenberg Photochemical Experiment (HOPE 2000): measurements and photostationary state calculations ofOH and peroxy radicals. Atmos. Chem. Phys. 3, 1565–1588.
Hiller, R.V., Neininger, B., Brunner, D., Gerbig, C., Bretscher, D., Künzle, T., Buchmann, N., Eugster, W., 2014. Aircraft-based CH4 flux estimates for validation of emissions from an agriculturally dominated area in Switzerland. J. GEOPHYS. RES-ATMOS. 119, 4874–4887.
Hood, C., MacKenzie, I., Stocker, J., Johnson, K., Carruthers, D., Vieno, M., Doherty, R., 2018. Air quality simulations for London using a coupled regional-to-local modelling system. Atmos. Chem. Phys. 18, 11221–11245.
Huang, T., Zhu, X., Zhong, Q., Yun, X., Meng, W., Li, B., Ma, J., Zeng, E.Y., Tao, S., 2017. Spatial and Temporal Trends in Global Emissions of Nitrogen Oxides from 1960 to 2014. Environ. Sci. Technol. 51, 7992–8000.
Huangfu, Y., Yuan, B., He, X., Liu, Z., Zhang, Y., Karl, T., Striednig, M., Ding, Y., Chen, X., Li, H., Zheng, H., Chang, M., Wang, X., Shao, M., 2024. Natural gas leakage ratio determined from flux measurements of methane in urban Beijing. Environ. Sci. Technol. Lett. 11, 1025–1031.
Jiang, Z., Zhu, R., Miyazaki, K., McDonald, B.C., Klimont, Z., Zheng, B., Boersma, K.F., Zhang, Q., Worden, H., Worden, J.R., Henze, D.K., Jones, D.B.A., Denier van der Gon, H.A.C., Eskes, H., 2022. Decadal variabilities in tropospheric nitrogen oxides over United States, Europe, and China. J. GEOPHYS. RES-ATMOS. 127.
Karl, T., Christian, L., Martin, G., Alexander, C., Martin, T., Arellano, J.V.-G.d., David, G., Lenschow, D., 2023. High urban NOx triggers a substantial chemical downward flux of ozone. Sci. Adv. 9, eadd2365.
Karl, T., Graus, M., Striednig, M., Lamprecht, C., Hammerle, A., Wohlfahrt, G., Held, A., von der Heyden, L., Deventer, M.J., Krismer, A., Haun, C., Feichter, R., Lee, J., 2017. Urban eddy covariance measurements reveal significant missing NOx emissions in Central Europe. Sci. Rep. 7.
Kemball-Cook, S., Yarwood, G., Johnson, J., Dornblaser, B., Estes, M., 2015. Evaluating NOx emission inventories for regulatory air quality modeling using satellite and air quality model data. Atmos. Environ. 117, 1–8.
Khalil, M.A.K., 2018. Steady states and transport processes in urban ozone balances. npj Clim. Atmos. Sci. 1.
Kim, N.K., Kim, Y.P., Morino, Y., Kurokawa, J.-i., Ohara, T., 2013. Verification of NOx emission inventory over South Korea using sectoral activity data and satellite observation of NO2 vertical column densities. Atmos. Environ. 77, 496–508.
Kim, S., Kim, D., Hong, H., Chang, L.-S., Lee, H., Kim, D.-R., Kim, D., Yu, J.-A., Lee, D., Jeong, U., Song, C.-K., Kim, S.-W., Park, S.S., Kim, J., Hanisco, T.F., Park, J., Choi, W., Lee, K., 2023. First-time comparison between NO2 vertical columns from Geostationary Environmental Monitoring Spectrometer (GEMS) and Pandora measurements. Atmos. Meas. Tech. 16, 3959–3972.
Klein, F., Platt, S.M., Farren, N.J., Detournay, A., Bruns, E.A., Bozzetti, C., Daellenbach, K.R., Kilic, D., Kumar, N.K., Pieber, S.M., Slowik, J.G., Temime-Roussel, B., Marchand, N., Hamilton, J.F., Baltensperger, U., Prévôt, A.S.H., El Haddad, I., 2016. Characterization of gas-phase organics using proton transfer reaction time-of-flight mass spectrometry: cooking emissions. Environ. Sci. Technol. 50, 1243–1250.
Kljun, N., Calanca, P., Rotach, M.W., Schmid, H.P., 2015. A simple two-dimensional parameterisation for Flux Footprint Prediction (FFP). Geosci. Model Dev. (GMD) 8, 3695–3713.
Kong, H., Lin, J., Chen, L., Zhang, Y., Yan, Y., Liu, M., Ni, R., Liu, Z., Weng, H., 2022. Considerable unaccounted local sources of NOx emissions in China revealed from satellite. Environ. Sci. Technol. 56, 7131–7142.
Korea Environmental Satellite Center (KESC), 2021. Geostationary environmental monitoring spectrometer. https://nesc.nier.go.kr/en/html/satellite/viewer/index.do.
Lamsal, L.N., Krotkov, N.A., Celarier, E.A., Swartz, W.H., Pickering, K.E., Bucsela, E.J., Gleason, J.F., Martin, R.V., Philip, S., Irie, H., Cede, A., Herman, J., Weinheimer, A., Szykman, J.J., Knepp, T.N., 2014. Evaluation of OMI operational standard NO2 column retrievals using in situ and surface-based NO2 observations. Atmos. Chem. Phys. 14, 11587–11609.
Lebel, E.D., Finnegan, C.J., Ouyang, Z., Jackson, R.B., 2022. Methane and NOx emissions from natural gas stoves, cooktops, and ovens in residential homes. Environ. Sci. Technol. 56, 2529–2539.
Lee, J.D., Helfter, C., Purvis, R.M., Beevers, S.D., Carslaw, D.C., Lewis, A.C., Moller, S.J., Tremper, A., Vaughan, A., Nemitz, E.G., 2015. Measurement of NOx fluxes from a tall tower in Central London, UK and comparison with emissions inventories. Environ. Sci. Technol. 49, 1025–1034.
Li, M., Liu, H., Geng, G., Hong, C., Liu, F., Song, Y., Tong, D., Zheng, B., Cui, H., Man, H., Zhang, Q., He, K., 2017. Anthropogenic emission inventories in China: a review. Natl. Sci. Rev. 4, 834–866.
Lin, X., Yang, R., Zhang, W., Zeng, N., Zhao, Y., Wang, G., Li, T., Cai, Q., 2023. An integrated view of correlated emissions of greenhouse gases and air pollutants in China. Carbon. Balance. Manage. 18, 9.
Liu, C., Shi, K., 2021. A review on methodology in O3-NOx-VOC sensitivity study. Environ. Pollut. 291, 118249.
Liu, F., Zhang, Q., van der A, R.J., Zheng, B., Tong, D., Yan, L., Zheng, Y., He, K., 2016. Recent reduction in NOx emissions over China: synthesis of satellite observations and emission inventories. Environ. Res. Lett. 11, 114002.
Liu, M., Lin, J., Kong, H., Boersma, K.F., Eskes, H., Kanaya, Y., He, Q., Tian, X., Qin, K., Xie, P., Spurr, R., Ni, R., Yan, Y., Weng, H., Wang, J., 2020. A new TROPOMI product for tropospheric NO2 columns over East Asia with explicit aerosol corrections. Atmos. Meas. Tech. 13, 4247–4259.
Lorente, A., Folkert Boersma, K., Yu, H., Dörner, S., Hilboll, A., Richter, A., Liu, M., Lamsal, L.N., Barkley, M., De Smedt, I., Van Roozendael, M., Wang, Y., Wagner, T., Beirle, S., Lin, J.-T., Krotkov, N., Stammes, P., Wang, P., Eskes, H.J., Krol, M., 2017. Structural uncertainty in air mass factor calculation for NO2 and HCHO satellite retrievals. Atmos. Meas. Tech. 10, 759–782.
Ma, Y., Lu, K., Chou, C.C.K., Li, X., Zhang, Y., 2017. Strong deviations from the NO-NO2-O3 photostationary state in the Pearl River Delta: indications of active peroxy radical and chlorine radical chemistry. Atmos. Environ. 163, 22–34.
Mao, S., Xu, L., Felipe, R., 2025. The evolution of diesel heavy-duty vehicles in China, 2012–2023. https://theicct.org/publication/evolution-diesel-hdv-china-2012-2023-feb25/#:~:text=This%20report%20analyzes%20China%27s%20heavy-duty%20vehicle%20industry%20between,the%20market%20for%20fuel%20supply%20and%20transmission%20technologies.
Marr, L.C., Moore, T.O., Klapmeyer, M.E., Killar, M.B., 2013. Comparison of NOx fluxes measured by Eddy covariance to emission inventories and land use. Environ. Sci. Technol. 47, 1800–1808.
Matthews, B., Schume, H., 2022. Tall tower eddy covariance measurements of CO2 fluxes in Vienna, Austria. Atmos. Environ. 274, 118941.
Mo, Z., Huang, S., Yuan, B., Pei, C., Song, Q., Qi, J., Wang, M., Wang, B., Wang, C., Li, M., Zhang, Q., Shao, M., 2020. Deriving emission fluxes of volatile organic compounds from tower observation in the Pearl River Delta. China. Sci. Total Environ. 741, 139763.
National Bureau of Statistics of China (NBSC), 2024. Number of civil motor vehicles ownership. https://data.stats.gov.cn/easyquery.htm?cn=E0103.
Nussbaumer, C.M., Place, B.K., Zhu, Q., Pfannerstill, E.Y., Wooldridge, P., Schulze, B.C., Arata, C., Ward, R., Bucholtz, A., Seinfeld, J.H., Goldstein, A.H., Cohen, R.C., 2023. Measurement report: airborne measurements of NOx fluxes over Los Angeles during the RECAP-CA 2021 campaign. Atmos. Chem. Phys. 23, 13015–13028.
Oke, T.a.M. G., 2017. Urban Climates. Cambridge university press.
Pfannerstill, E.Y., Arata, C., Zhu, Q., Schulze, B.C., Woods, R., Harkins, C., Schwantes, R. H., McDonald, B.C., Seinfeld, J.H., Bucholtz, A., Cohen, R.C., Goldstein, A.H., 2023. Comparison between spatially resolved airborne flux measurements and emission inventories of volatile organic compounds in Los Angeles. Environ. Sci. Technol. 57, 15533–15545.
Plake, D., Sörgel, M., Stella, P., Held, A., Trebs, I., 2015. Influence of meteorology and anthropogenic pollution on chemical flux divergence of the NO–NO2–O3 triad above and within a natural grassland canopy. Biogeosciences 12, 945–959.
Rinne, J., Markkanen, T., Ruuskanen, T.M., Petäjä, T., Keronen, P., Tang, M.J., Crowley, J.N., Rannik, Ü., Vesala, T., 2012. Effect of chemical degradation on fluxes of reactive compounds – a study with a stochastic Lagrangian transport model. Atmos. Chem. Phys. 12, 4843–4854.
Shaw, M.D., Lee, J.D., Davison, B., Vaughan, A., Purvis, R.M., Harvey, A., Lewis, A.C., Hewitt, C.N., 2015. Airborne determination of the temporo-spatial distribution of benzene, toluene, nitrogen oxides and ozone in the boundary layer across Greater London, UK. Atmos. Chem. Phys. 15, 5083–5097.
Song, M., Zhao, X., Liu, P., Mu, J., He, G., Zhang, C., Tong, S., Xue, C., Zhao, X., Ge, M., Mu, Y., 2023. Atmospheric NOx oxidation as major sources for nitrous acid (HONO). npj Clim. Atmos. Sci. 6, 30.
Squires, F.A., Nemitz, E., Langford, B., Wild, O., Drysdale, W.S., Acton, W.J.F., Fu, P., Grimmond, C.S.B., Hamilton, J.F., Hewitt, C.N., Hollaway, M., Kotthaus, S., Lee, J., Metzger, S., Pingintha-Durden, N., Shaw, M., Vaughan, A.R., Wang, X., Wu, R., Zhang, Q., Zhang, Y., 2020. Measurements of traffic-dominated pollutant emissions in a Chinese megacity. Atmos. Chem. Phys. 20, 8737–8761.
Stockwell, C.E., Bela, M.M., Coggon, M.M., Gkatzelis, G.I., Wiggins, E., Gargulinski, E.M., Shingler, T., Fenn, M., Griffin, D., Holmes, C.D., Ye, X., Saide, P.E., Bourgeois, I., Peischl, J., Womack, C.C., Washenfelder, R.A., Veres, P.R., Neuman, J.A., Gilman, J. B., Lamplugh, A., Schwantes, R.H., McKeen, S.A., Wisthaler, A., Piel, F., Guo, H., Campuzano-Jost, P., Jimenez, J.L., Fried, A., Hanisco, T.F., Huey, L.G., Perring, A., Katich, J.M., Diskin, G.S., Nowak, J.B., Bui, T.P., Halliday, H.S., DiGangi, J.P., Pereira, G., James, E.P., Ahmadov, R., McLinden, C.A., Soja, A.J., Moore, R.H., Hair, J.W., Warneke, C., 2022. Airborne emission rate measurements validate

remote sensing observations and emission inventories of Western U.S. wildfires. Environ. Sci. Technol. 56, 7564–7577.
Tadic, I., Crowley, J.N., Dienhart, D., Eger, P., Harder, H., Hottmann, B., Martinez, M., Parchatka, U., Paris, J.-D., Pozzer, A., Rohloff, R., Schuladen, J., Shenolikar, J., Tauer, S., Lelieveld, J., Fischer, H., 2020. Net ozone production and its relationship to nitrogen oxides and volatile organic compounds in the marine boundary layer around the Arabian Peninsula. Atmos. Chem. Phys. 20, 6769–6787.
UK Environmental Agency (UKEA), 2024. Air quality statistics in the UK, 1987 to 2023 - nitrogen dioxide (NO2). https://www.gov.uk/government/statistics/air-quality-statistics/ntrogen-dioxide.
van Geffen, J., Eskes, H., Compernolle, S., Pinardi, G., Verhoelst, T., Lambert, J.-C., Sneep, M., ter Linden, M., Ludewig, A., Boersma, K.F., Veefkind, J.P., 2022. Sentinel-5P TROPOMI NO2 retrieval: impact of version v2.2 improvements and comparisons with OMI and ground-based data. Atmos. Meas. Tech. 15, 2037–2060.
Vaughan, A.R., Lee, J.D., Misztal, P.K., Metzger, S., Shaw, M.D., Lewis, A.C., Purvis, R. M., Carslaw, D.C., Goldstein, A.H., Hewitt, C.N., Davison, B., Beevers, S.D., Karl, T. G., 2016. Spatially resolved flux measurements of NOxfrom London suggest significantly higher emissions than predicted by inventories. Faraday. Discuss. 189, 455–472.
Verhoelst, T., Compernolle, S., Pinardi, G., Lambert, J.-C., Eskes, H.J., Eichmann, K.-U., Fjæraa, A.M., Granville, J., Niemeijer, S., Cede, A., Tiefengraber, M., Hendrick, F., Pazmiño, A., Bais, A., Bazureau, A., Boersma, K.F., Bognar, K., Dehn, A., Donner, S., Elokhov, A., Gebetsberger, M., Goutail, F., Grutter de la Mora, M., Gruzdev, A., Gratsea, M., Hansen, G.H., Irie, H., Jepsen, N., Kanaya, Y., Karagkiozidis, D., Kivi, R., Kreher, K., Levelt, P.F., Liu, C., Müller, M., Navarro Comas, M., Piters, A.J.M., Pommereau, J.-P., Portafaix, T., Prados-Roman, C., Puentedura, O., Querel, R., Remmers, J., Richter, A., Rimmer, J., Rivera Cárdenas, C., Saavedra de Miguel, L., Sinyakov, V.P., Stremme, W., Strong, K., Van Roozendael, M., Veefkind, J.P., Wagner, T., Wittrock, F., Yela González, M., Zehner, C., 2021. Ground-based validation of the Copernicus Sentinel-5P TROPOMI NO2 measurements with the NDACC ZSL-DOAS, MAX-DOAS and Pandonia global networks. Atmos. Meas. Tech. 14, 481–510.
Vuolo, R.M., Loubet, B., Mascher, N., Gueudet, J.-C., Durand, B., Laville, P., Zurfluh, O., Ciuraru, R., Stella, P., Trebs, I., 2017. Nitrogen oxides and ozone fluxes from an oilseed-rape management cycle: the influence of cattle slurry application. Biogeosciences 14, 2225–2244.
Wang, S., Xing, J., Chatani, S., Hao, J., Klimont, Z., Cofala, J., Amann, M., 2011. Verification of anthropogenic emissions of China by satellite and ground observations. Atmos. Environ. 45, 6347–6358.
Wang, T., Xue, L., Brimblecombe, P., Lam, Y.F., Li, L., Zhang, L., 2017. Ozone pollution in China: a review of concentrations, meteorological influences, chemical precursors, and effects. Sci. Total Environ. 575, 1582–1596.
Xu, T., Zhang, C., Xue, J., Hu, Q., Xing, C., Liu, C., 2023. Estimating hourly nitrogen oxide emissions over east Asia from geostationary satellite measurements. Environ. Sci. Technol. Lett. 11, 122–129.
Yang, B., Zhang, K.M., Xu, W.D., Zhang, S., Batterman, S., Baldauf, R.W., Deshmukh, P., Snow, R., Wu, Y., Zhang, Q., Li, Z., Wu, X., 2018a. On-Road chemical transformation as an important mechanism of NO2 Formation. Environ. Sci. Technol. 52, 4574–4582.
Yang, W., Zhang, Q., Wang, J., Zhou, C., Zhang, Y., Pan, Z., 2018b. Emission characteristics and ozone formation potentials of VOCs from gasoline passenger cars at different driving modes. Atmos. Pollut. Res. 9, 804–813.
Zhao, Y., Xia, Y., Zhou, Y., 2018a. Assessment of a high-resolution NOX emission inventory using satellite observations: a case study of southern Jiangsu, China. Atmos. Environ. 190, 135–145.
Zhao, Y., Xia, Y., Zhou, Y., 2018b. Assessment of a high-resolution NOX emission inventory using satellite observations: a case study of southern Jiangsu, China. Atmos. Environ. 190, 135–145.
Zheng, B., Tong, D., Li, M., Liu, F., Hong, C., Geng, G., Li, H., Li, X., Peng, L., Qi, J., Yan, L., Zhang, Y., Zhao, H., Zheng, Y., He, K., Zhang, Q., 2018. Trends in China's anthropogenic emissions since 2010 as the consequence of clean air actions. Atmos. Chem. Phys. 18, 14095–14111.
Zhu, Q., Place, B., Pfannerstill, E.Y., Tong, S., Zhang, H., Wang, J., Nussbaumer, C.M., Wooldridge, P., Schulze, B.C., Arata, C., Bucholtz, A., Seinfeld, J.H., Goldstein, A.H., Cohen, R.C., 2023. Direct observations of NOx emissions over the San Joaquin Valley using airborne flux measurements during RECAP-CA 2021 field campaign. Atmos. Chem. Phys. 23, 9669–9683.